Summary of Thesis

SYNTHESIS AND OPTICAL PROPERTIES OF STRONTIUM PYROPHOSPHATE PHOSPHOR

A THESIS
SUBMITTED BY

NIMESH PRAFULBHAI PATEL

FOR THE AWARD OF THE DEGREE OF
DOCTOR OF PHILOSOPHY

IN
PHYSICS

UNDER THE GUIDANCE OF
Prof. M. SRINIVAS

PHYSICS DEPARTMENT
FACULTY OF SCIENCE
THE MAHARAJA SAYAJIRAO UNIVERSITY OF BARODA
VADODARA
FEBRUARY-2019

Pure and rare earth doped inorganic pyrophosphates gathered scientific and technological important because of their luminescent, dielectric, semiconductor, catalytic, magnetic, fluorescent, and ion-exchange properties [1-3]. A large variety of properties and corresponding applications is the reason, why the synthesis of inorganic pyrophosphates is a more attractive field of research for researchers. Out of many properties, luminescent properties are significantly investigated by many researchers. Wide-bandgap rare-earth doped inorganic pyrophosphate materials have gained much more attention, for their potential applications in diverse areas such as X- and gamma-radiation detectors, lighting, display phosphors, light-emitting diodes, scintillators, and solid state lasers, and because they are highly transparent, easily shaped, and cost-effective. In this thesis, Rare earth doped and co-doped strontium pyrophosphate by combustion synthesis method to investigate its luminescence properties and its application [4, 5].

The thesis comprises of six chapters. **Chapter 1 (Introduction)** comprises of the introduction to the research problem and its relevant literature review. **Chapter 2 (Experimental Method)** contains the basic information of combustion synthesis method and the procedure followed for the synthesis of phosphors. **Chapter 3 (Structural Characterization)** contains the fundamental details of the characterization techniques used to characterize the synthesized phosphor, experimental results and discussion of rare earth doped strontium pyrophosphate. **Chapter 4 (Photoluminescence of Strontium Pyrophosphate)** contains the basic information of photoluminescence (PL) and some significant experimental results and discussion of photoluminescence property of rare earth doped strontium pyrophosphate. **Chapter 5 (Thermoluminescence Strontium Pyrophosphate)** contains the basic information of thermoluminescence (TL) and experimental results and discussion of thermoluminescence property of rare earth doped strontium pyrophosphate after beta irradiation. The outcome of TL results has been discussed on the basis of theory and its application in detail.

Chapter 1 Introduction

A luminescent phosphor is a solid, which converts certain types of energy into electromagnetic radiation over and above thermal radiation [6, 7]. *The word phosphor means "light bearer" in Greek and appears in Greek myths as the personification of the morning star Venus* [8] [9, 10]. The luminescence from the phosphors can acquire by exciting the

phosphor in different excitation radiations such as UV and visible radiation (photoluminescence), a beam of energetic electrons (cathodoluminescence), x-rays (x-ray excited luminescence), etc [6, 11-14]. Thermoluminescence is one of the distinct ways to get luminescence, which is stimulation by the heating of luminescence, preliminary excited in a different way [15, 16]. Luminescence measures the energy levels of the luminescence centers formed inside the phosphors. The energy level of a luminescence center is defined as its characteristic state, which is related to the physical nature of the center and to the energetic and dynamic processes that the center undergoes [17, 18].

Rare earth doped inorganic luminescent materials are well known for emission in distinct wavelengths in the electromagnetic spectrum [19, 20]. The phosphors have a wide range of applications in the lighting devices such as cathode ray tubes (CRT), tri-phosphor fluorescent lamps, x-ray intensifying screens and newly developed vacuum mercury-free lamps [14, 21, 22]. It has other applications in a display such as plasma display panels and field emission displays. The momentous application of phosphors for light emitting diodes (LEDs) technology changes the history of the solid state lighting and has completely changed the "world of luminance" [19, 23, 24]. LEDs are significantly energy-efficient lighting device with a long lifetime.

Phosphates and pyrophosphates are the different condensed and polymeric form of mono-phosphoric acid [25]. Pyrophosphate is one type of the phosphorus oxyanion with general formula $P_2O_7^{4-}$ also called as diphosphate or di-polyphosphate [26]. The oxyanion is generally termed as $M_XO_Y^{Z-}$ (M = C, S, P, F; O - Oxygen). Oxyanions are designed from a large number of the chemical elements which can be banded with one or more than one oxygen atoms. Phosphate materials are categorized into three types of phosphates; (i) monophosphates, (ii) condensed phosphates, (iii) oxyphosphates. There are several pyrophosphates were developed for a various application that has the general formula of $A^{4+}P_2O_7$, $A^{2+}{}_2P_2O_7$, $A^{1+}B^{3+}P_2O_7$, $A^{1+}{}_2B^{1+}{}_2\ P_2O_7$, $A^{1+}{}_2B^{2+}P_2O_7$ and $A^{1+}{}_4P_2O_7$, where A and B are an inorganic atom.

There are many research articles published based on various inorganic pyrophosphates groups, where the synthesis and luminescence properties were investigated for a different application. All possible phase formation and effect of Eu doping on photoluminescence properties of CaP_2O_7 is investigated by Doat et al. [27]. UV spectral emission of HfP_2O_7 and

blue emission of Ti^{4+} doped HfP_2O_7 is investigated for their x-ray storage application by Schipper et al. [28]. The crystal structure and spectroscopic analysis as well as luminescence studies of $KErP_2O_7{\cdot}2H_2O$ were reported by Assaaoudi et al. [29]. Luminescence properties of Ce^{3+}-doped the first lutetium diphosphate $NH_4LuP_2O_7$ was shown by Li et al [5]. The investigation of the energy gap of ABP_2O_7 ($A = Na^+, Li^+$; $B = Al^{3+}, In^{3+}$) double phosphates from the electronic structure and the optical properties were reported by Hizhnyi et al [30]. UV-visible spectroscopic properties based on energy transfer occur in Ce^{3+} and Pr^{3+} doped $A^+RE^{3+}P_2O_7$ (A^+ = Na, K, Rb, Cs; RE^{3+} = Y, Lu) alkali rare earth diphosphates were investigated by Yuan et al [31]. The structural study of $LiFeP_2O_7$, $LiScP_2O_7$, and $NaScP_2O_7$ for conductivity measurement were reported by Kaepe et al [32].

From the literature survey, it is found that different inorganic pyrophosphates show good luminescent behavior. Out of different type of pyrophosphates, the majority were synthesized by solid-state method, a sol-gel method, wet precipitation method. There are very few research article in which the luminescent properties rare earth doped of strontium pyrophosphate were investigated. Therefore, strontium pyrophosphate is taken as a host material which is doped with different rare earth elements to enhance the luminescent properties of the host. The rare earth doped and co-doped strontium pyrophosphate was synthesized by combustion method which is the easiest method from the synthesis of efficient luminescent materials.

Chapter 2 Experimental Method

Combustion synthesis method generally called as self-propagating high-temperature synthesis, was discovered in the 1980s. It is mainly a wet-chemical processing method. It does not require additional calcination of the material and repetitive heating treatment. Combustion synthesis method was accidentally discovered by Prof. Patil in his laboratory in India in 1988 [33]. Combustion synthesis method is an efficient and inexpensive method for the production of highly crystalline materials like inorganic-ceramic phosphor, magnetic materials, etc [34, 35]. The crystalline materials can be prepared with controlled particle size specifically of the order of micrometre to nanometre, and having a composition to assemble them together into large frame of structures with extraordinary properties and different functions [36, 37]. It is an extensively useful method to develop materials in all section for commercial and industrial applications. It is one of the most popular method that draw attention from the scientists and

material technologists of various disciplines since last three decades. The physical properties like structure having crystalline or amorphous, purity of material, surface area, particle size, porosity and agglomeration of the synthesized powders which highly depends on the parameters adopted for the process [35, 38].

Commercially purchased pure analytical reagent grad precursors such as strontium carbonate, ammonium dihydrogen phosphate, cerium oxide, europium oxide, dysprosium oxide, terbium oxide, gadolinium oxide, erbium oxide, and samarium oxide were used for the synthesis of rare earth doped strontium pyrophosphate. Urea was used as a fuel for combustion in this method. The list of samples synthesized for Re^{3+} doped and co-doped $Sr_2P_2O_7$ phosphors are summarized in Table 2.1 and Table 2.2 respectively. Figure 2.2 shows the different steps of combustion synthesis method adopted for synthesis of rare earth doped $Sr_2P_2O_7$. In this method, different steps involved such as formation of mixture of precursors, grinding, heating treatment and grinding of obtained material after heating. The balanced chemical reaction for the synthesized phosphor is given below,

$$\mathbf{2\ SrCO_3 + 2\ (NH_4)_2HPO_4 \rightarrow Sr_2P_2O_7 + 3\ H_2O + 2\ CO_2 + 4\ NH_3}$$

Sample	Doping Ion Concentration (mol%)
$Sr_2P_2O_7$: x Ce^{3+}	x = 0.5, 1.0, 1.5, 2.0, 2.5
$Sr_2P_2O_7$: x Eu^{3+}	x = 0.5, 1.0, 1.5, 2.0, 2.5, 5.0
$Sr_2P_2O_7$: x Tb^{3+}	x = 0.5, 1.0, 1.5, 2.0, 2.5, 5.0
$Sr_2P_2O_7$: x Dy^{3+}	x = 0.5, 1.0, 1.5, 2.0, 2.5, 5.0
$Sr_2P_2O_7$: x Er^{3+}	x = 0.5, 1.0, 1.5, 2.0, 2.5, 5.0
$Sr_2P_2O_7$: x Gd^{3+}	x = 0.5, 1.0, 1.5, 2.0, 2.5, 5.0

Table 2.1 List of sample of single RE^{3+} doped $Sr_2P_2O_7$ synthesized for the study of its luminescence properties.

Sample	Doping Ion Concentration (mol%)
$Sr_2P_2O_7$: x Ce^{3+}, y Eu^{3+}	x = 1.0, y = 1.0
$Sr_2P_2O_7$:x Ce^{3+}, y Tb^{3+}	x = 1.0, y = 1.0
$Sr_2P_2O_7$: x Ce^{3+}, y Dy^{3+}	x = 1.0, y = 1.0
$Sr_2P_2O_7$: x Ce^{3+}, y Er^{3+}	x = 1.0, y = 1.0
$Sr_2P_2O_7$: x Ce^{3+}, y Gd^{3+}	x = 1.0, y = 1.0
$Sr_2P_2O_7$: x Ce^{3+}, y Sm^{3+}	x = 1.0, y = 1.0
$Sr_2P_2O_7$: x Ce^{3+}, y Nd^{3+}	x = 1.0, y = 1.0

Table 2.2 List of sample of double rare earth doped $Sr_2P_2O_7$ synthesized for the study of its luminescence properties.

Ce^{3+}-doped $Sr_2P_2O_7$ phosphors were synthesized by the combustion method for different concentrations namely 0.5, 1.0, 1.5, 2.0 and 2.5 mol%. The phosphors were synthesized from the precursors $SrCO_3$ (A.R.), $(NH_4)_2HPO_4$ (A.R.), Ce_2O_3 (99.99%) (A.R.) and urea. The precursors were taken as per the stoichiometric ratio considered from the balanced chemical equation. Urea was used as a fuel at a ratio 15% of the total mass of the mass of precursors. The precursors were grinded in mortar pastel for 30 minute to obtain homogeneous mixture. The homogeneous mixture was transferred into alumina crucible and put inside the muffle furnace for heat treatment at 1200°C for 3 hour at atmospheric pressure. After heating treatment, the furnace was allowed to cool naturally to the room temperature. All prepared samples were in the pure white powder form. The samples were grinded in a mortar–pestle for half hour to obtain the homogeneous fine powder form [39]. Similar procedure is been followed for RE^{3+} co-doped $Sr_2P_2O_7$ phosphors. All phosphors were successfully synthesized in pure powder form.

Chapter 3 Structural Characterization

The synthesized phosphors were first characterized by X-ray diffractometer (XRD, Bruker D8; Cu Ka radiation, λ = 0.15406 nm, 40 kV and 40 mA) to examine crystal phase formation and structural parameters of phosphors. The XRD measurements were carried out for diffraction angle of 2θ values of 10°–60° in steps of 0.02°/s. Fourier transform infrared (FTIR) spectra of the samples were recorded by FTIR-4100 type A IR spectrometer in transmittance mode in wavenumber range of 400–4000 cm^{-1}. The surface morphologies of phosphors were obtained by field emission scanning electronic microscope (FE-SEM, JSM-7500F).

X-ray Diffraction

XRD patterns of pure $Sr_2P_2O_7$ and JCPDS: 24-1011 are shown in Figure 3.1. The XRD patterns of $Sr_2P_2O_7$: x Ce^{3+} (x = 0.5, 1.0, 1.5, 2.0, 2.5 mol%) are shown in Figure 3.2(A). The XRD patterns of rare earth doped $Sr_2P_2O_7$ samples are compared with JCPDS standard card no. 24-1011. The hkl parameters of the prepared samples are similar to that of the JCPDS standard card no. 24-1011 of α-$Sr_2P_2O_7$ that indicates the existence of a pure single-phase α-$Sr_2P_2O_7$. The structural parameters of the samples were analyzed using powder software for XRD analysis. The analysis confirms that the samples have a pure α-phase with crystallization in the orthorhombic structure and space group of P_{nam}. The doping of various rare earth ions and their percentage concentration does not make any perceptible variation in XRD patterns as well as no other peaks found than that of $Sr_2P_2O_7$ in these patterns. This indicates that the prepared samples are single phased and substitution of Sr^{2+} by RE^{3+} does not cause any substantial modification in the crystal structure of host. Some prominent intense peaks are observed in the XRD patterns at different 2θ values of 12.12°, 25.95°, 26.27°, 26.93°, 33.16°, 33.63° and 44.40° corresponding to the (110), (201), (031), (211), (002), (141) and (232) planes for these host lattice respectively. Sharp intense peaks in the XRD patterns of all rare earth doped samples signify that all samples are polycrystalline material. The calculated crystalline parameters of Ce^{3+} doped $Sr_2P_2O_7$ phosphors are summarized in Table 3.1. All RE^{3+} doped $Sr_2P_2O_7$ phosphors shows similar kind of nature as that of Ce^{3+} doped $Sr_2P_2O_7$ phosphors. The diffraction peaks of a powder XRD pattern of $Sr_2P_2O_7$ are very sharp because of high crystallinity. The average crystallite size of rare earth doped $Sr_2P_2O_7$ phosphors were calculated by using the Scherrer's formula and Williamson-Hall (W–H) plot analysis. The

magnified XRD pattern for 2θ range 25°-35° is shown in Figure 3.2 (B). It is noted that there is minute shifting in peak position towards higher diffraction angle 2θ for the increment of doping concentration. The peak shifting towards higher 2θ value is observed in XRD pattern due to the increase in the doping concentrations revealed that the more number of substitution of doping occurs at the place of Sr^{2+} site in host lattice. The shifting in peak position ensues due to decrease in unit cell size which can results due to the ionic radii difference of host ion Sr^{2+} and rare earth ion RE^{3+}.

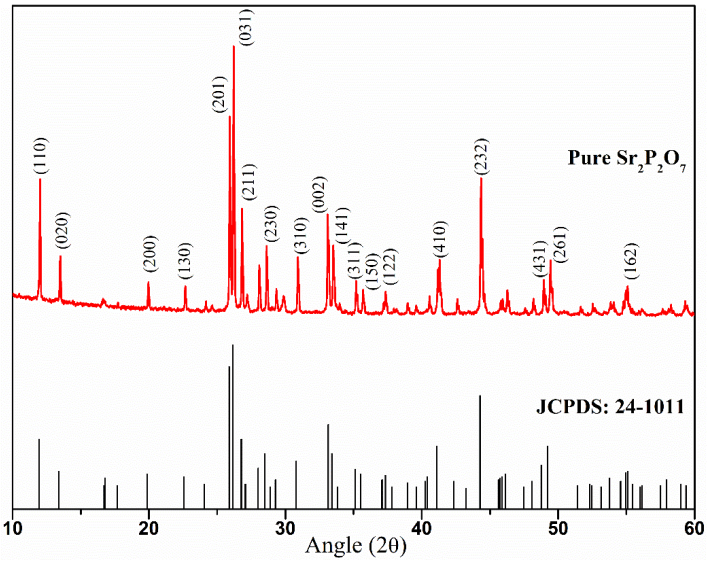

Figure 3.1 XRD patterns of pure $Sr_2P_2O_7$ and JCPDS: 24-1011.

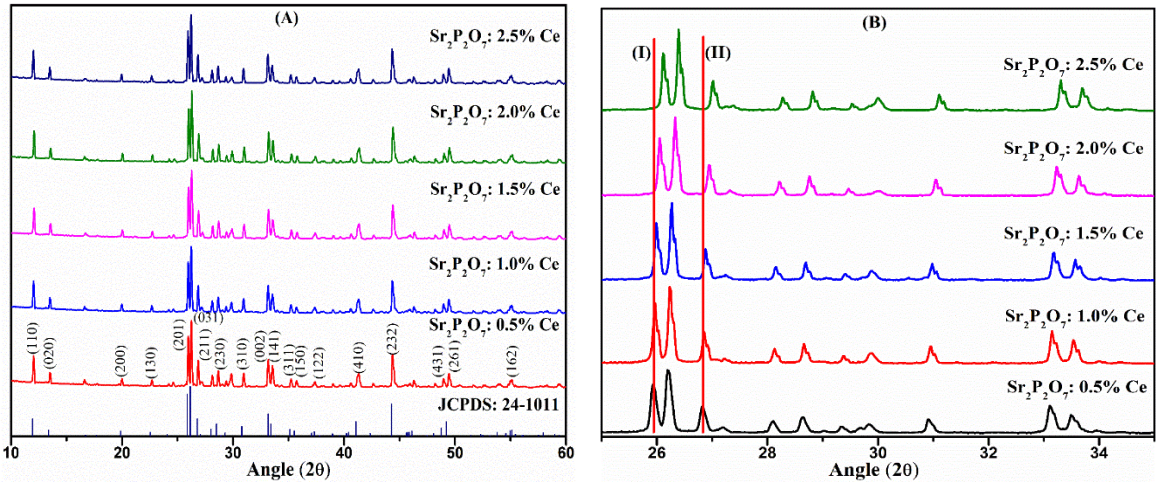

Figure 3.2 (A) XRD patterns of $Sr_2P_2O_7$: x Ce^{3+} (x = 0.5, 1.0, 1.5, 2.0 and 2.5 mol%) phosphor and JCPDs Card No. 24-1011. (B) Magnified XRD patterns.

Sample	Lattice Parameter			Volume of Unit Cell 'V' (Å ^{3})
	a (Å)	b (Å)	c (Å)	
$Sr_2P_2O_7$: 0.5 mol% Ce^{3+}	8.984	13.193	5.451	646.08
$Sr_2P_2O_7$: 1.0 mol% Ce^{3+}	8.976	13.185	5.447	644.64
$Sr_2P_2O_7$: 1.5 mol% Ce^{3+}	8.865	13.176	5.441	635.53
$Sr_2P_2O_7$: 2.0 mol% Ce^{3+}	8.861	13.167	5.437	634.34
$Sr_2P_2O_7$: 2.5 mol% Ce^{3+}	8.854	13.156	5.431	632.62

Table 3.1 Crystal structure parameters of $Sr_2P_2O_7$: x Ce^{3+} (x = 0.1, 0.5, 1.0, 1.5, 2.0 and 2.5 mol%).

Samples →	$Sr_2P_2O_7$: Ce^{3+}	$Sr_2P_2O_7$: Eu^{3+}	$Sr_2P_2O_7$: Tb^{3+}	$Sr_2P_2O_7$: Dy^{3+}	$Sr_2P_2O_7$: Er^{3+}	$Sr_2P_2O_7$: Gd^{3+}
Doping Concentration ↓	Crystallite Size (nm)					
0.5 mol%	82.55	72.83	69.46	68.29	61.54	71.53
1.0 mol%	81.40	71.97	----	----	60.13	70.17
1.5 mol%	79.21	70.47	----	66.69	58.84	69.99
2.0 mol%	78.19	68.93	----	----	57.35	67.82
2.5 mol%	77.54	68.04	65.79	63.53	55.87	66.38
5.0 mol%	----	65.89	63.65	----	----	----

Table 3.2 Crystallite Size of $Sr_2P_2O_7$: RE (RE = Ce^{3+}, Eu^{3+}, Tb^{3+}, Dy^{3+}, Er^{3+} Gd^{3+}) calculated through Scherrer's formula.

The crystallite size calculated from to different methods are summarized in Table 3.2 and Table 3.3. It suggest that the crystallite size decreases as the doping concentration RE^{3+} increases, which suggest that the incorporation of doing ion increases as at higher temperature. All RE^{3+} co-doped $Sr_2P_2O_7$ phosphors also shows similar type of nature.

Samples →	$Sr_2P_2O_7$: Ce^{3+}	$Sr_2P_2O_7$: Eu^{3+}	$Sr_2P_2O_7$: Tb^{3+}	$Sr_2P_2O_7$: Dy^{3+}	$Sr_2P_2O_7$: Er^{3+}	$Sr_2P_2O_7$: Gd^{3+}
Doping Concentration ↓	**Crystallite Size (nm)**					
0.5 mol%	88.62	79.32	78.67	81.38	72.37	85.33
1.0 mol%	86.78	76.93	----	----	69.59	82.27
1.5 mol%	85.11	74.87	----	76.90	68.25	79.19
2.0 mol%	83.43	71.82	----	----	64.95	74.62
2.5 mol%	80.76	70.14	70.58	71.47	61.53	72.43
5.0 mol%	----	68.92	67.54	----	----	----

Table 3.2 Crystallite Size of $Sr_2P_2O_7$: RE (RE = Ce^{3+}, Eu^{3+}, Tb^{3+}, Dy^{3+}, Er^{3+} Gd^{3+}) calculated trough Williamson-Hall plot analysis.

FTIR

FTIR transmittance spectra of synthesized $Sr_2P_2O_7$: x Ce^{3+} (x = 0.5, 1.0, 1.5, 2.0, 2.5 mol%) is shown in Figure 3.3. The FTIR spectra of phosphors were recorded for the wavenumber range from 400 – 4000 cm^{-1}, the fingerprint region of the FTIR spectra of the range 400–2000 cm^{-1} has been demonstrated in the graph. All FTIR spectra were recorded from the KBr pellet of $Sr_2P_2O_7$. The KBr pellet for all samples were prepared for 99:1% ratio of KBr to $Sr_2P_2O_7$. The thickness of each pellet is approximately maintained up to 1 mm which has semi-transparent nature. Various transmittance bands of pyrophosphate group and phosphate group are observed in the FTIR spectra. FTIR spectra of the phosphors show the evidence of the multiple vibrational bands. The pyrophosphate group $(P_2O_7)^{4-}$ could be the form of O_3P-O-PO_3, and can be attributed to an assembly of the vibration modes of the PO_3 groups and the P-O-P groups. The formation of the $P_2O_7^{4-}$ modes in the phosphor is conceded on the basis of the PO_3 and P-O-P vibrations. The phosphor prepared for different concentrations of doping ion, exhibit sharp bands in the region of wavenumber 1200–400 cm^{-1}. The FTIR spectra of $Sr_2P_2O_7$: x RE (x = 0.5, 1.0, 1.5, 2.0, 2.5 and 5.0 mol%; RE = Ce^{3+}, Eu^{3+}, Tb^{3+}, Dy^{3+}, Er^{3+}, Gd^{3+}) were consistent for all samples and there is no change in peak position. The FTIR results it is found that the formation of phosphors were consistent and having uniform crystal phase formation as analyzed in x-ray diffraction.

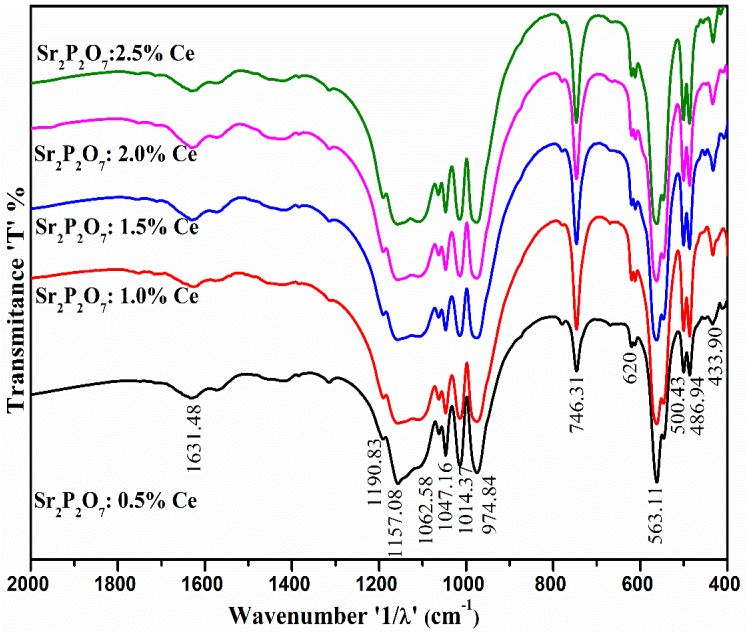

Figure 3.3 FTIR spectra of $Sr_2P_2O_7$: x Ce^{3+} (x = 0.5, 1.0, 1.5, 2.0 and 2.5 mol%).

SEM

The particle size and surface of the phosphors is significantly more important criterion for the commercial applications of the phosphors in solid state lighting. The phosphors having micron particles size and smooth surface can be feed well the commercial demand for WLEDs and lamp phosphors. Figure 3.4 (A), (B) shows the SEM images of $Sr_2P_2O_7$: 0.5 mol% Eu^{3+} and Figure 3.4 (C), (D) shows SEM images of $Sr_2P_2O_7$: 2.0 mol% Eu^{3+} synthesized at 1200 °C annealing temperatures. Figure 3.23 (E) shows the part unagglomerate particles in Figure 3.23 (A) of $Sr_2P_2O_7$: 2.0% Eu^{3+}, which could be appear like the shape of a capsule. The powder form of Eu^{3+} doped $Sr_2P_2O_7$ materializes in highly crystalline form with uneven morphology observed under different resolution and the average grain size of 2 – 3 μm. It is observed that the crystallites particles having nonuniform shape with evolved boundary of submicron size and strongly agglomerated. It could be occur due to the non-uniform temperature distribution during the firing of material by flux during synthesis. The surface morphology of the particles is smooth for both concentrations of doping which could be observed due to melting occurred at the surfaces of certain particles at high temperature.

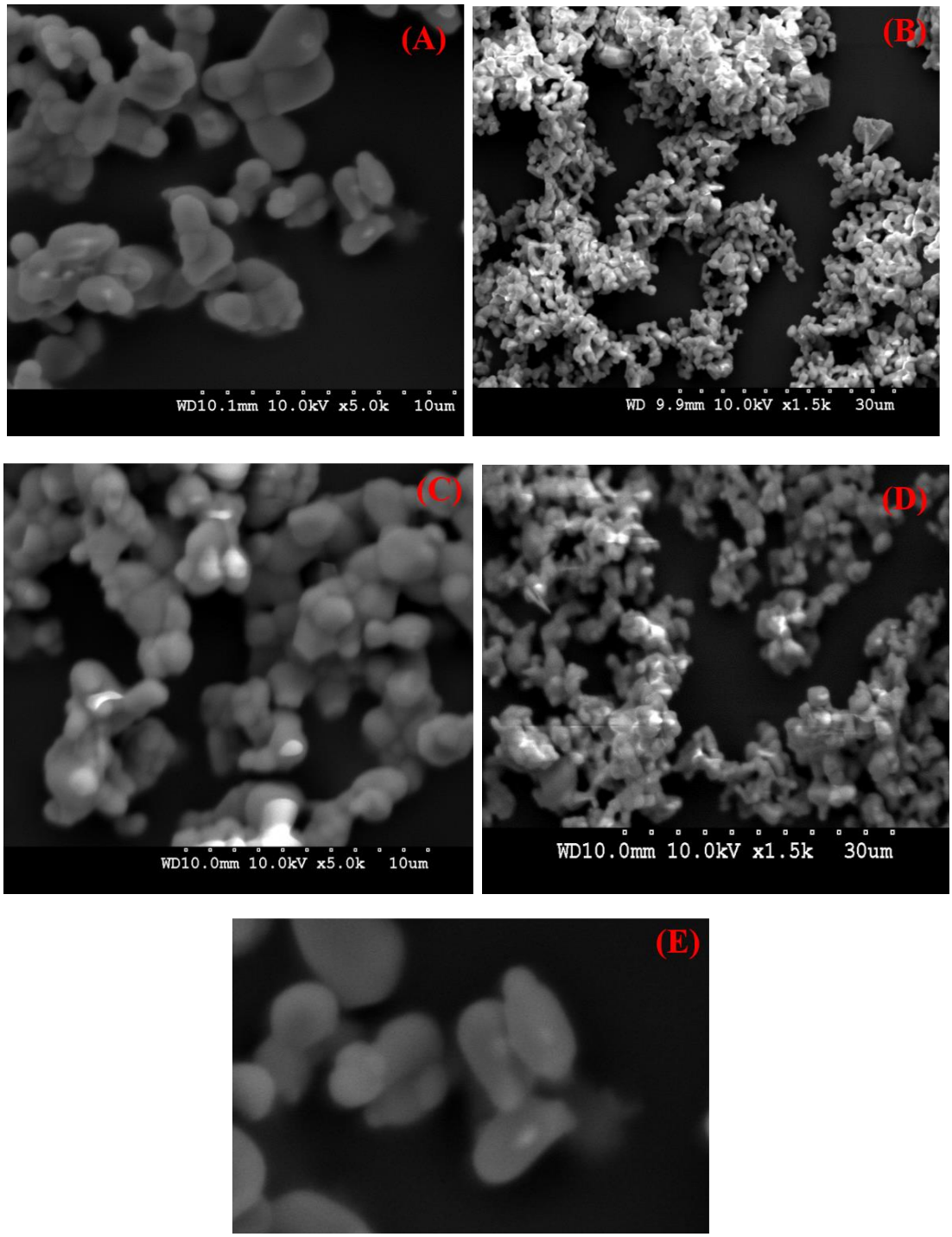

Figure 3.4 SEM images; (A), (B) Sr_2P_{27}: 1.0 mol% Eu^{3+}; (C), (D) $Sr_2P_2O_7$: 2.5 mol% Eu^{3+}.

Chapter 4 Photoluminescence of Strontium Pyrophosphate

There are several RE^{3+} doped $Sr_2P_2O_7$ phosphors were analyzed for the PL study, here only the best result has been explained.

PL of $Sr_2P_2O_7$: Eu^{3+}

Figure 4.1 shows the excitation spectra of $Sr_2P_2O_7$: x Eu^{3+} (x = 0.5, 1.0, 1.5, 2.0, 2.5 and 5.0 mol%) recorded at 618 nm emission wavelength at room temperature. The excitation spectra consist of a broad band and some sharp lines in the UV-Blue range 350-500 nm. The excitation spectra of the phosphor show predominant excitation under the $^5D_0$-$^7F_2$ (618 nm) emission of Eu^{3+} ions and it can remain constant for all doping concentration. The excitation intensity is been prominent for the high concentration of 5.0 mol% Eu^{3+}, it reveals absorption of incident photons increases with the increase in doping concentration. The broad band centered at 266 nm could be attributed due to the charge-transfer transition band of doping ion and oxygen ion of the host lattice (Eu^{3+}-O^2) [40]. The energy of the charge transfer state (CTS) essentially depends on the environments of host surrounding the doping ion. The energies of CTS and 4f states of trivalent rare earth ion are the relatively same for rare-earth ions in any host materials.

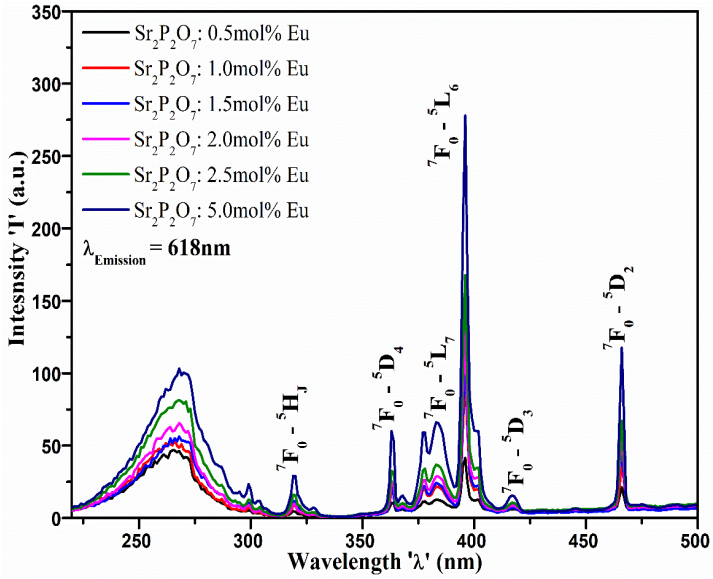

Figure 4.1 Excitation spectra of $Sr_2P_2O_7$: x Eu^{3+} (x = 0.5, 1.0, 1.5, 2.0, 2.5 and 5.0 mol%) phosphor.

As shown in Figure 4.1, the broad band excitation with maximum peak intensity at 266 nm is occurred due to CTS, where the charge transfer from host Sr^{2+} to dopant Eu^{3+}. The energy of excitation peak is 37.6×10^3 cm^{-1} and it is comparable to that of the energy of commercial phosphor 40×10^3 cm^{-1}. As a result, CTS interact with 4f states and it can lead to f-f emissions [9]. The excitation spectra contain discrete sharp lines due to the characteristic

4f–4f transitions of Eu^{3+} ion at 396 nm ($^7F_0$-$^5L_6$) and 466 nm ($^7F_0$-$^5D_2$) indicating that $Sr_2P_2O_7$: Eu^{3+} can be efficiently excited by UV-blue LED (350–480 nm) and blue-LED chips (465 nm). The excitation spectra also contain several small excitation lines ascribed due to the $^7F_0$-$^5D_4$ (363 nm), $^7F_0$-$^5L_7$ (383 nm), and $^7F_0$-$^5D_3$ (417 nm) transitions of Eu^{3+} ions. The phosphors for LED application should be excited in the range of the near violet-blue region of the excitation spectra [41, 42]. The prominent red-emitting UV-LED phosphor exhibit absorption at 395 nm (i.e., LED excitation wavelength) are potential for orange-red LED.

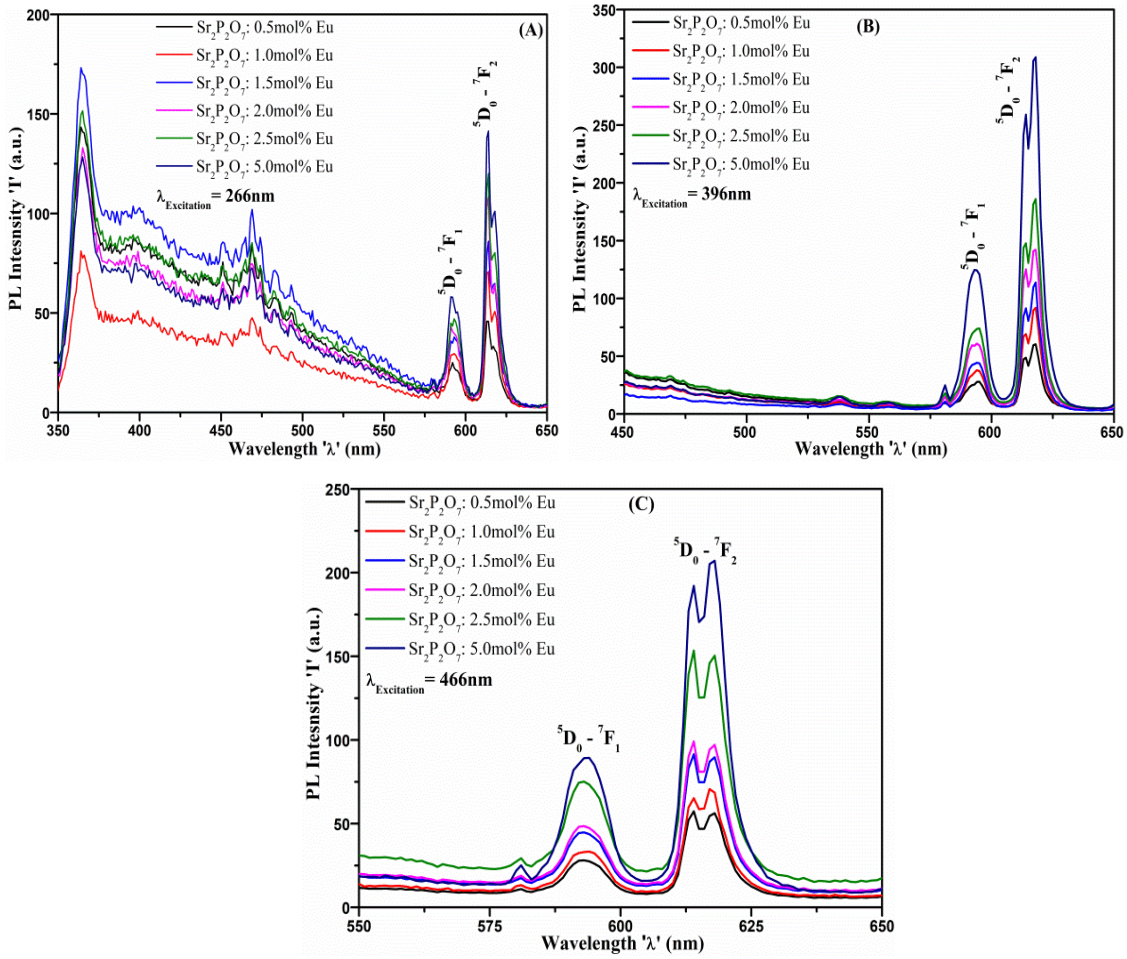

Figure 4.2 PL emission spectra: (A) $\lambda_{Excitation}$= 266 nm; (B) $\lambda_{Excitation}$= 396 nm; (B) $\lambda_{Excitation}$= 466nm, of $Sr_2P_2O_7$: x Eu^{3+} (x = 0.5, 1.0, 1.5, 2.0, 2.5 and 5.0 mol%) phosphor.

The PL emission spectra of $Sr_2P_2O_7$: x% Eu^{3+} measured upon the excitation wavelength 266 nm, 396 nm and 466 nm are shown in Figure. 4.2 (A), (B), (C) respectively. The PL emission spectra for excitation wavelength 396 nm (Figure. 4.2 (A)) contain strong

PL emission peak observed for different excitations is located at 618 nm, attributed to the $^5D_0$-$^7F_2$ characteristic transition of Eu^{3+} ion and the weak PL emission peak at 595 nm is attributed to the $^5D_0$-$^7F_1$ transitions of Eu^{3+} due to the $4f^6$ configuration [42, 43].

The PL emission spectra of $Sr_2P_2O_7$: x% Eu^{3+} for excitation wavelength 466 nm and 266 nm are not as much intense than that of 396 nm (Figure. 4.2 (B), (C)), as well as the PL emission intensity of characteristic transitions of Eu^{3+} is mainly depends upon the doping concentration of Eu^{3+} in host $Sr_2P_2O_7$. The behavior of Eu^{3+} ion in the phosphor is hypersensitive to the local chemical environment according to the Judd–Ofelt theory [44-46]. The site symmetry of Eu^{3+} ion inside the microstructures of host lattice has an influence on the luminescence efficiency of Eu^{3+}-activated hosts. The magnetic dipole transition ($^5D_0$-$^7F_1$) is significant when Eu^{3+} ion occupies an inversion symmetry site in host $Sr_2P_2O_7$ i.e., centrosymmetric in the host lattice. The electric-dipole transition ($^5D_0$-$^7F_2$) is significant when Eu^{3+} ion in the host is subjected without an inversion center i.e., non-centrosymmetric in host lattice.

PL of $Sr_2P_2O_7$: 1.0 mol% Ce^{3+}, 1.0 mo% Eu^{3+}

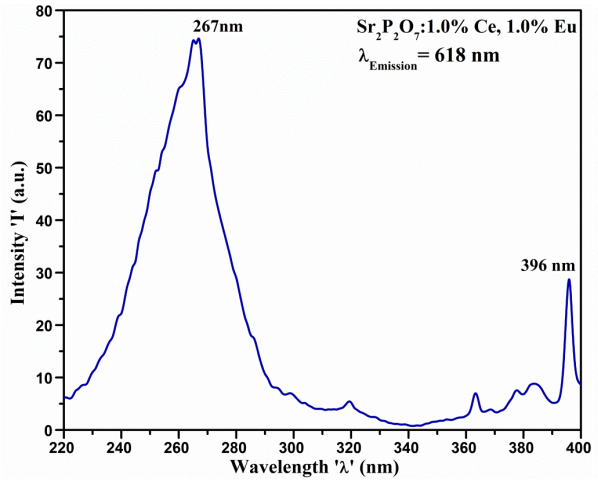

Figure 4.3 PL excitation spectra of 0.1mol% Ce^{3+}, 0.1mol% Eu^{3+}doped $Sr_2P_2O_7$ phosphor.

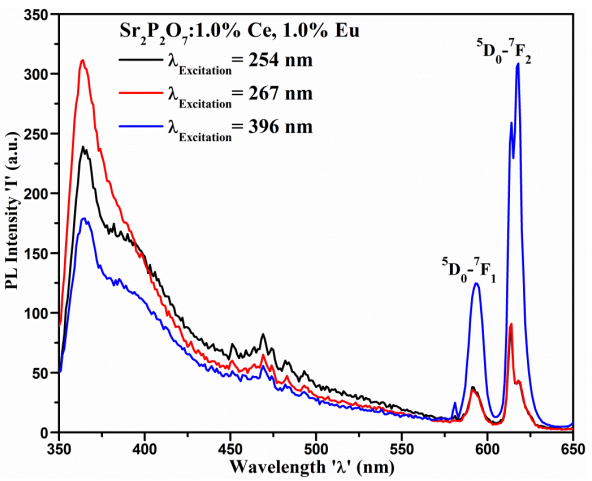

Figure 4.4 PL emission spectra of 1.0mol% Ce^{3+}, 1.0mol% Eu^{3+}doped $Sr_2P_2O_7$ phosphor.

Figure 4.3 shows the excitation spectra of Ce^{3+}-Eu^{3+} co-doped $Sr_2P_2O_7$ phosphors monitored at 618 nm emission wavelength. The excitation spectrum of the phosphor monitored at emission wavelength 618 nm consists of two broad bands centered at 267 nm

and a small peak 396 nm. The broad peak centered at 267 nm is derived due to the 4f – 5d transition of Ce^{3+} and small peak centered at 396 nm is derived due to the characteristic 4f–4f transitions of Eu^{3+} ion ascribed by the $^7F_0 - {}^5L_6$ transition. It is reported that the energy transfer from Ce^{3+} ion to Eu^{3+} does not take place or very weak because Ce^{3+} ion having the lowest fourth ionization potential and Eu^{3+} ion having the highest third ionization potential in terms of the stability of completely- and half-filled shells. Figure 4.4 shows the PL emission spectra of Ce^{3+}-Eu^{3+} co-doped $Sr_2P_2O_7$ phosphors monitored at 254, 267 and 396 nm excitation wavelength. It is observed, the weak interaction between Ce^{3+} and Eu^{3+} causes the reduction in UV-blue emission of Ce^{3+}. Under 396 nm excitation, PL emission spectra show strong emission at 621 nm attributed to the $^5D_0$-$^7F_2$ characteristic transition of Eu^{3+} ion and at 595 nm is attributed to the $^5D_0$-$^7F_1$ transitions of Eu^{3+} ion. Under 254 and 276 nm excitation, PL emission due Ce^{3+} and Eu^{3+} reduced sharply may come about to the more number of nonradiative transition take place at that excitation.

Chapter 5 Thermoluminescence of Strontium Pyrophosphate

There are several RE^{3+} doped $Sr_2P_2O_7$ phosphors were analyzed for the PL study, here only the best result has been explained.

TL of $Sr_2P_2O_7$: Eu^{3+}

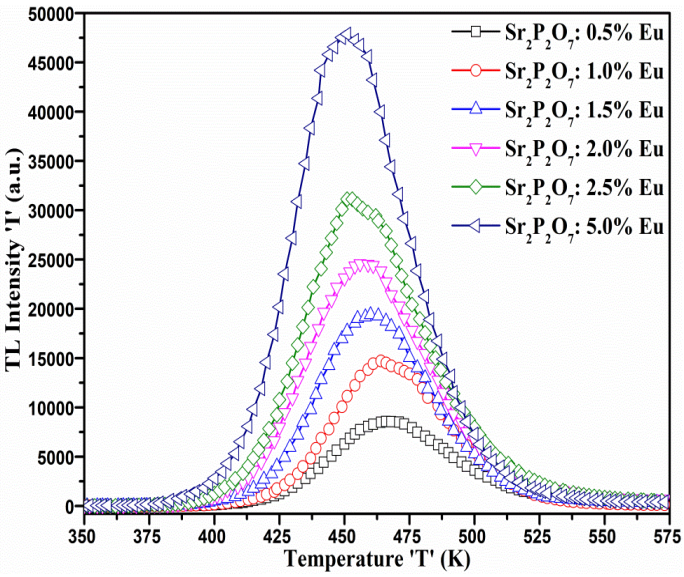

Figure 5.1 TL glow curve of $Sr_2P_2O_7$: x Eu^{3+} (x = 0.5, 1.0, 1.5, 2.0, 2.5, 5.0 mol%) phosphors irradiated by β-radiation for 5 minute of 0.48 Gy dose.

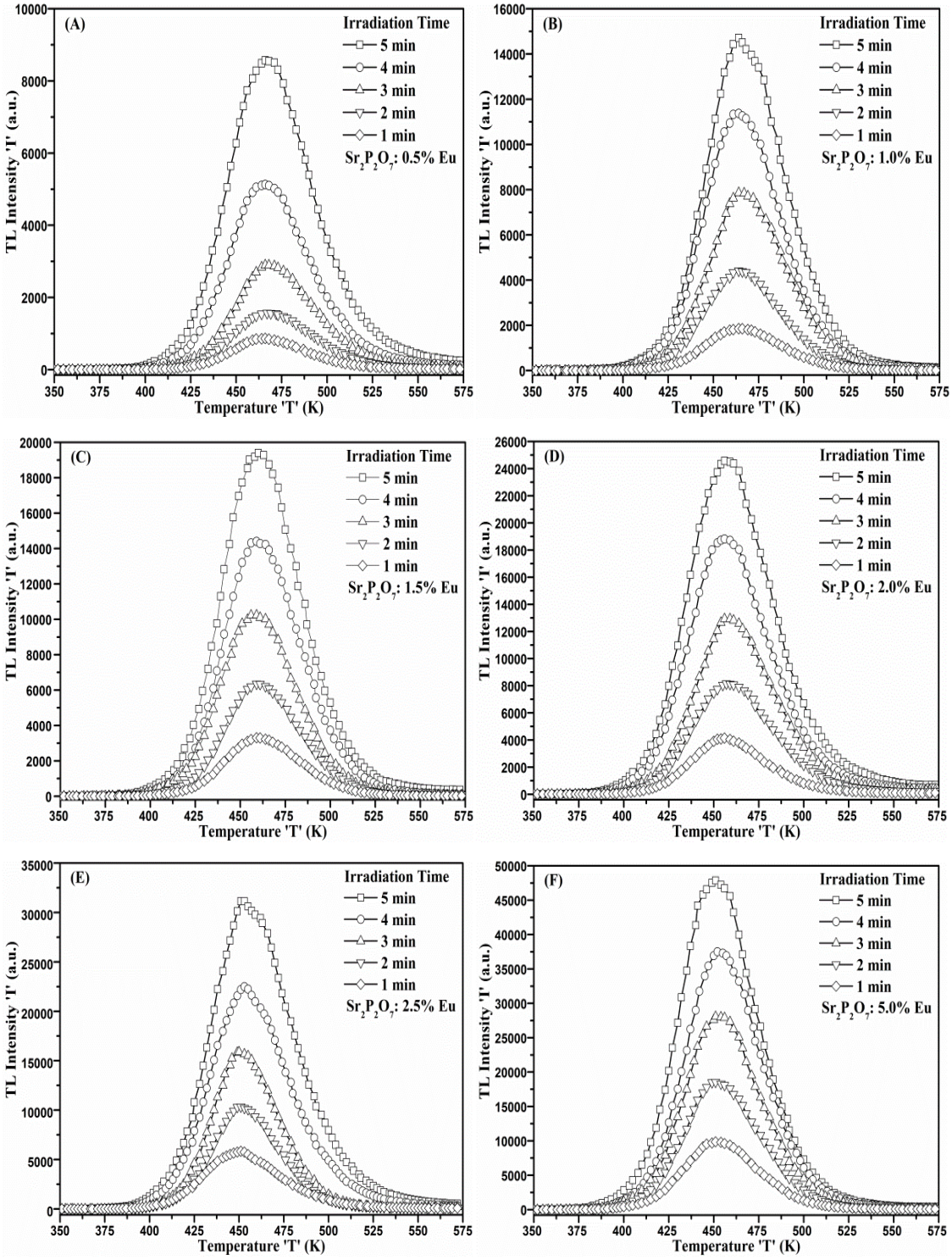

Figure 5.2 TL glow curve for various time of β-irradiation: (A) $Sr_2P_2O_7$: 0.5 mol% Eu^{3+}; (B) $Sr_2P_2O_7$: 1.0 mol% Eu^{3+}; (C) $Sr_2P_2O_7$: 1.5 mol% Eu^{3+}; (D) $Sr_2P_2O_7$: 2.0 mol% Eu^{3+}; (E) $Sr_2P_2O_7$: 2.5 mol% Eu^{3+}; (F) $Sr_2P_2O_7$: 5.0 mol% Eu^{3+}.

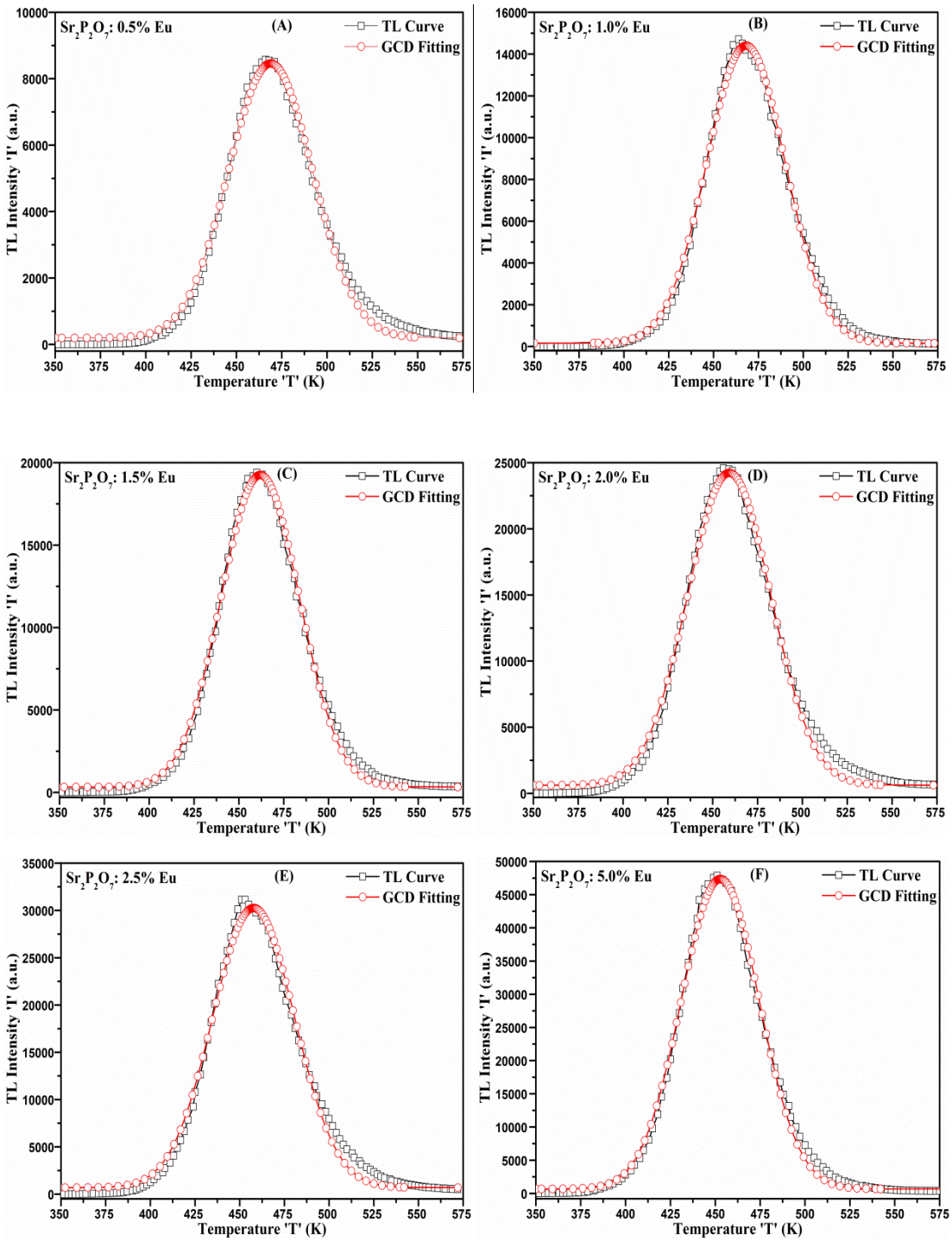

Figure 5.3 GCD fitting of TL glow curves of (A) $Sr_2P_2O_7$: 0.5 mol% Eu^{3+}; (B) $Sr_2P_2O_7$: 1.0 mol% Eu^{3+}; (C) $Sr_2P_2O_7$: 1.5 mol% Eu^{3+}; (D) $Sr_2P_2O_7$: 2.0 mol% Eu^{3+}; (E) $Sr_2P_2O_7$: 2.5 mol% Eu^{3+}; (F) $Sr_2P_2O_7$: 5.0 mol% Eu^{3+}.

In general observation TL study, it is found that the TL intensity of phosphor is significantly depends on the doping concentration and the radiation dose absorbed by

phosphors. Figure 5.1 shows the TL glow curves of Eu^{3+} doped $Sr_2P_2O_7$ irradiated by β-radiation for 5 min. It shows the TL glow curve intensity increases as the concentration of doping increases, while the peak position shifting toward the higher temperature for lower concentration. TL glow curves of Eu^{3+} doped $Sr_2P_2O_7$ phosphor consists of single bell shape curves. The highest intensity exhibits at 452 K temperature for 5.0 mol% Eu^{3+} doped $Sr_2P_2O_7$ and 467 K for 0.5 mol% Eu^{3+} doped $Sr_2P_2O_7$ which signify that the position of electron trap cent are changes with doping concentration.

Figure 5.2 shows the TL glow curves of Eu^{3+} doped $Sr_2P_2O_7$ carried out after β-irradiation of phosphors by 5 mCi Sr^{90} β-source for different irradiation time, i.e., 0.097 to 0.48 Gy. It shows the TL intensity increases with β-dose that revealed the number electrons trapped at luminescence centers formed in energy gap. TL parameters of glow of glow such as activation energy, frequency factor, order of kinetics involve in TL mechanism and life time has been calculated by different methods. Figure 5.3 shows the GCD fitting of TL glows of Eu^{3+} doped $Sr_2P_2O_7$ phosphors recorded after 5 minute β- radiation dose. Precise values of figure of merit (FOM) were calculated using equation (16) for experimental and theoretically fitted glow curves. The calculated values of figure of merit (FOM) for different fitted glow curves are mentioned in Table 5.1, which signifies the appropriate fitting of experimental glow curves. GCD fitting of the glow curves have been done through the Kitis et al. equation of second order kinetics given by equation (15). The GCD fitting of the glow curve reveal that the glow curves of 0.5 – 5.0 mol% Eu^{3+} $Sr_2P_2O_7$ follows the second order kinetics, which can identified from the values of order of kinetics 'b' in this method mentioned in Table 5.1. The values of order of kinetics 'b' for each fitted curves are about 1.8 – 2.0, which is the value of second order kinetics. The consistent values of activation energy 'E_a' and frequency factor 's' for electron trap centre in Eu^{3+} doped $Sr_2P_2O_7$ phosphor obtained through GCD method are summarized in Table 5.1. For Eu^{3+} doped $Sr_2P_2O_7$ phosphors the activation energy 'E_a' are ranging from 1.17 – 1.23 eV and frequency factor 's' are of the order of 10^{11} s^{-1}.

Sample	Activation Energy 'Ea' (eV)	Order Of Kinetics 'b'	FOM %	Frequency Factor 's' (s^{-1})
$Sr_2P_2O_7$: 0.5 mol% Eu^{3+}	1.21±0.03	1.8	0.07	3.17×10^{11}
$Sr_2P_2O_7$: 1.0 mol% Eu^{3+}	1.23±0.04	1.9	1.4	1.07×10^{11}
$Sr_2P_2O_7$: 1.5 mol% Eu^{3+}	1.20±0.03	2.0	0.8	2.36×10^{11}
$Sr_2P_2O_7$: 2.0 mol% Eu^{3+}	1.17±0.02	2.0	0.2	1.00×10^{11}
$Sr_2P_2O_7$: 2.5 mol% Eu^{3+}	1.18±0.04	2.0	0.9	3.17×10^{11}
$Sr_2P_2O_7$: 5.0 mol% Eu^{3+}	1.21±0.02	1.9	2.5	2.51×10^{11}

Table 5.1 Summary of TL kinetic parameters of glow curve for sample Eu^{3+} doped $Sr_2P_2O_7$ irradiated by β-radiation for 5 minute of 0.48 Gy dose calculated by GCD method.

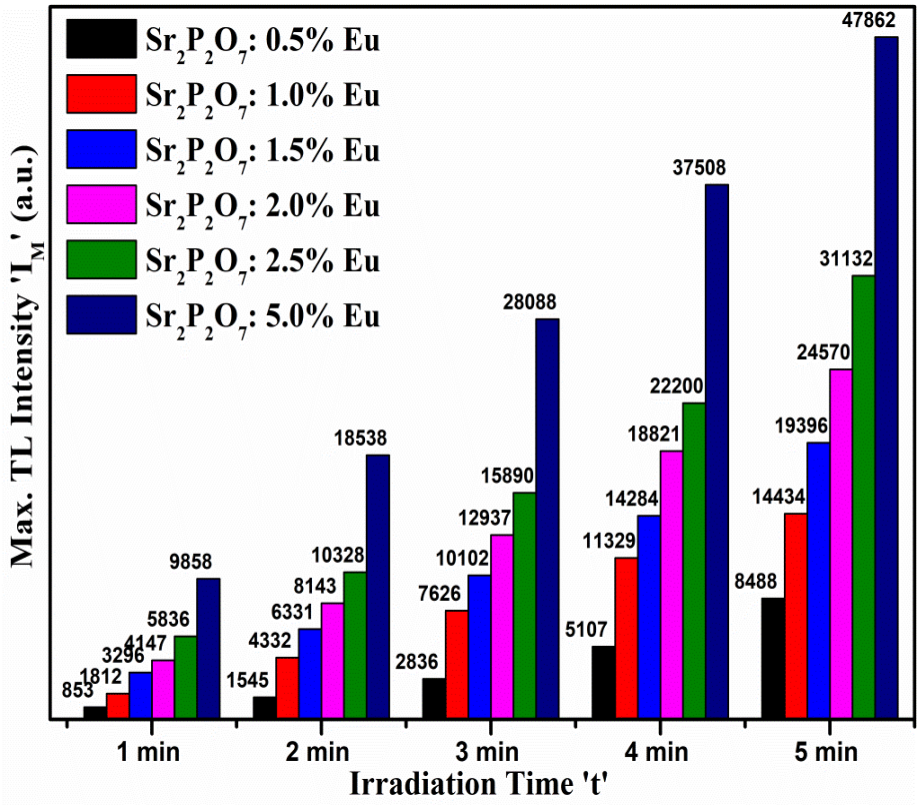

Figure 5.4 Maximum TL intensity 'I_M' vs β-irradiation time 't' graph of Eu^{3+} doped $Sr_2P_2O_7$ irradiated by β-radiation for 5 minute of 0.48 Gy dose.

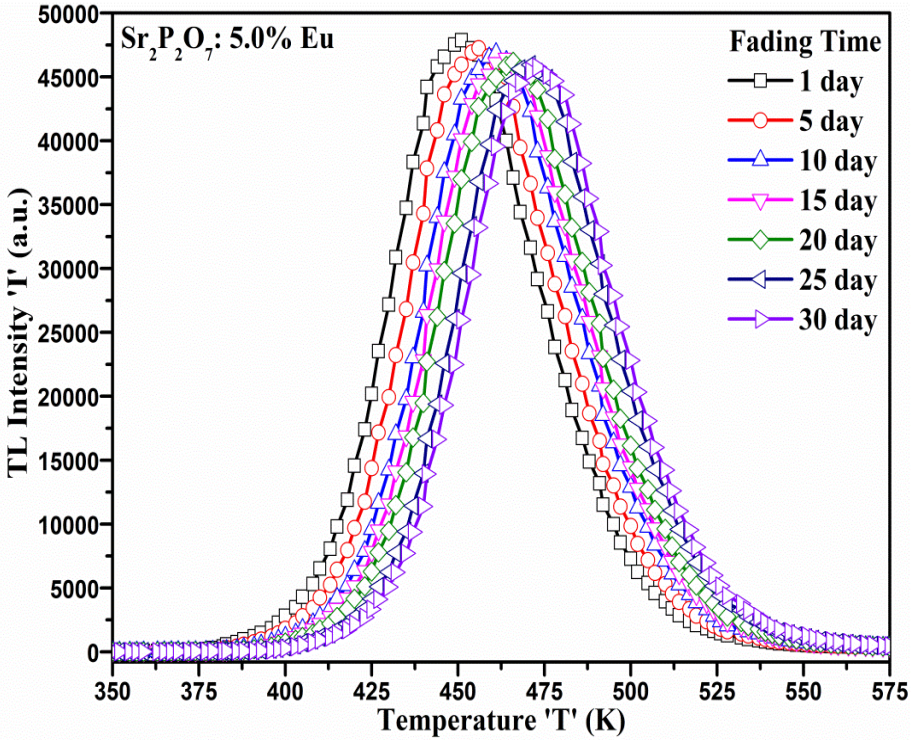

Figure 5.5 TL glow curve of 5.0 mol% Eu^{3+} doped $Sr_2P_2O_7$ for fading time irradiated by β-radiation for 5 minute of 0.48 Gy dose.

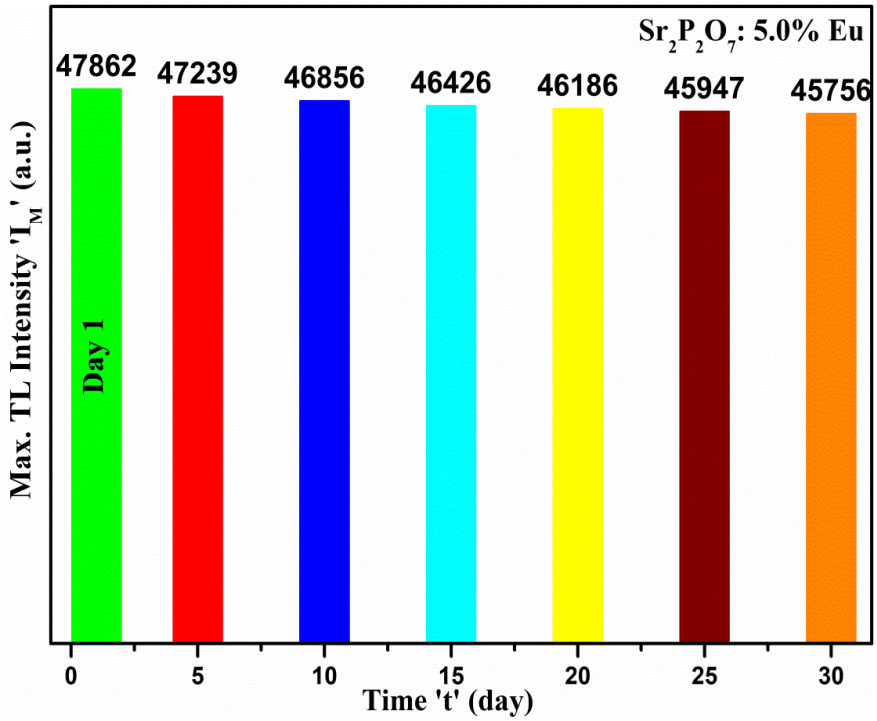

Figure 5.6 Maximum TL intensity 'I_M' vs Fading time 't' graph of 5.0 mol% Eu^{3+} doped $Sr_2P_2O_7$ phosphor irradiated by β-radiation for 5 minute of 0.48 Gy dose.

Figure 5.4 shows Maximum TL intensity vs β-irradiation time graph of Eu^{3+} doped $Sr_2P_2O_7$ for different concentrations of doping ion. The amount of radiation dose and the concentration of dopant prominently affect the TL emission because both the way the trap of electron induced considerably. In Eu^{3+} doped $Sr_2P_2O_7$, it is found that the TL emission intensify as the dose of radiation and doping concentration increase as illustrated in Figure 5.4. TL response after different doses shows linear with β-dose and doping concentration. Figure 5.5 shows the TL glow curve of $Sr_2P_2O_7$: 5.0 mol% Eu^{3+} phosphor recorded at different time after β- irradiation of phosphor for 5 minute to examine the fading effect after exposure, which gives the information about how long the phosphor can store the exposure energy. The fading effect is the one of the most useful characteristic of good TL dosimeter. The TL glow curves were acquired to analyze the fading effect of TL glow curve for one month at interval of five days for one month for all samples. The phosphors were stored in dark condition at room temperature after exposure of β-radiation. This fading study showed that the TL glow curve peak temperature 450 K is shifted towards higher temperature up to 465 K in the time period of one month, but the fading of Peak maximum is much low. Similar kind of fading effect were observed in all samples with different concentration and doses. Figure 5.6 shows Maximum TL intensity vs Fading time graph of $Sr_2P_2O_7$: 5.0% Eu^{3+} phosphor irradiated by β- radiation for 5 minute.

Chapter 6 Conclusion

Synthesized phosphors were characterized with different technique which signifies the formation of pure single phase of $Sr_2P_2O_7$.

Photoluminescence of above mentioned results are as below:

- Eu^{3+} doped $Sr_2P_2O_7$ phosphor was excited under it major excitation wavelength of 396 and 466 nm. The PL emission occur at 618 nm which is a red emission useful for LED applications. PL emission intensifications with increases in doping concentration, the maximum intensity of 618 nm emission peak for the 5.0 mol% Eu^{3+} is increased by 5-6 time than that of the 0.5 mol% Eu^{3+}. The PL emission also depends on the crystallite sized, for Eu^{3+} doped $Sr_2P_2O_7$ phosphor the PL intensity increase with decrease in

crystallite size. The PL emission results of Eu^{3+} doped $Sr_2P_2O_7$ phosphor suggest its potential application for wLED under blue excitation.

- 1.0 mol% Ce^{3+}, 1.0 mol% Eu^{3+} doped $Sr_2P_2O_7$ phosphor shows prominent 618 nm red emission under the excitation wavelength 396 nm. The emission under the excitation wavelength 254 and 268 nm shows weak emission due to the weak interaction between the Ce^{3+} and Eu^{3+} ions. Therefore, Eu^{3+} reduces the Ce^{3+} emission. This phosphor gives light red emission under 396 nm excitation.

Thermoluminescence of above mentioned results are as below:

- RE^{3+} doped $Sr_2P_2O_7$ phosphors, Eu^{3+} doped phosphor showed maximum TL intensity of about 45000 units, which is a good TL outcome. TL glow curve intensity of RE^{3+} doped $Sr_2P_2O_7$ phosphors increases linearly with doping concentration and exposure dose. The fading of the TL intensity is very low for the storage of 30 day, which is less than 7%. The reusability of the phosphor were studied for ten cycles, which is consistent for each use for exposure. All the phosphors are very sensitive to the lower doses. The TL parameters obtained for different RE^{3+} doped $Sr_2P_2O_7$ phosphors are very consistent and nearby the traditional TLDs. The results suggests that the RE^{3+} doped phosphors may be the potential for environmental dosimetry and accidental dosimetry applications.

References

1. Yazici, A.N., et al., *Thermoluminescent properties of $Sr_2P_2O_7$ doped with copper and some rare earth elements.* Journal of Luminescence, 2010. **130**(10): p. 1744-1749.
2. Ferid, M., K. Horchani, and J. Amami, *Preparation, structure and infrared spectrum of $NaEuP_2O_7$.* Materials research bulletin, 2004. **39**(12): p. 1949-1955.
3. Guler, H. and F. Kurtulus, *A microwave-assisted route for the solid-state synthesis of lead pyrophosphate, $Pb_2P_2O_7$.* Journal of materials science, 2005. **40**(24): p. 6565-6569.
4. Withers, R., et al., *A new three-dimensional incommensurately modulated cubic phase (in Zr P_2O_7) and its symmetry characterization via temperature-dependent electron diffraction.* Journal of Solid State Chemistry, 2001. **157**(1): p. 186-192.
5. Li, M.R., et al., *Low-Temperature Flux Synthesis, Crystal Structure and Ce-Doped Luminescence of the First Lutetium Diphosphate $NH_4Lu\ P_2O_7$.* European journal of inorganic chemistry, 2005. **2005**(23): p. 4693-4696.

6. Blasse, G. and B. Grabmaier, *A General Introduction to Luminescent Materials*, in *Luminescent materials*, 1994, Springer. p. 1-9.
7. Edgar, A., *Luminescent Materials*, in *Springer Handbook of Electronic and Photonic Materials*2017, Springer. p. 1-1.
8. Dexter, D.L., *A theory of sensitized luminescence in solids.* The Journal of Chemical Physics, 1953. **21**(5): p. 836-850.
9. Shionoya, S., W.M. Yen, and H. Yamamoto, *Phosphor handbook*, 2006: CRC press.
10. Yen, W.M. and H. Yamamoto, *Fundamentals of phosphors*, 2006: CRC press.
11. Singh, D., et al., *Recent Advancements in Luminescent Materials and Their Potential Applications.* Advanced Magnetic and Optical Materials, 2016: p. 317-352.
12. Fonda, G.R., *Luminescent material*, 1950, Google Patents.
13. Blasse, G., *Chemistry and physics of R-activated phosphors.* Handbook on the physics and chemistry of rare earths, 1979. **4**: p. 237-274.
14. Blasse, G. and B. Grabmaier, *Luminescent materials*, 2012: Springer Science & Business Media.
15. Richter, D., *Advantages and limitations of thermoluminescence dating of heated flint from Paleolithic sites.* Geoarchaeology, 2007. **22**(6): p. 671-683.
16. Rhodes, E.J., *Optically stimulated luminescence dating of sediments over the past 200,000 years.* Annual Review of Earth and Planetary Sciences, 2011. **39**: p. 461-488.
17. Gaft, M., R. Reisfeld, and G. Panczer, *Modern luminescence spectroscopy of minerals and materials*, 2015: Springer.
18. Boyn, R., *4f–4f Luminescence of Rare-Earth Centers in II–VI Compounds.* physica status solidi (b), 1988. **148**(1): p. 11-47.
19. Ye, S., et al., *Phosphors in phosphor-converted white light-emitting diodes: Recent advances in materials, techniques and properties.* Materials Science and Engineering: R: Reports, 2010. **71**(1): p. 1-34.
20. Shinde, K.N., et al., *Basic mechanisms of photoluminescence*, in *Phosphate Phosphors for Solid-State Lighting*2012, Springer. p. 41-59.
21. Murthy, K., *Nano phosphors for light emitting diodes (LEDs) Syntheses and Characterization.* Recent Research in Science and Technology, 2012. **4**(8).
22. Li, Y.Q., *Structure and luminescence properties of novel rare-earth doped silicon nitride based materials*, 2005: Technische Universiteit Eindhoven.
23. Lin, C.C. and R.-S. Liu, *Advances in phosphors for light-emitting diodes.* The journal of physical chemistry letters, 2011. **2**(11): p. 1268-1277.
24. Horng, R.-H., et al., *Solid-state lighting with high brightness, high efficiency, and low cost.* International Journal of Photoenergy, 2014. **2014**.
25. r se Averbuch-Pouchot, M.-T. and A. Durif, *Topics in phosphate chemistry*, 1996: World Scientific.
26. Baker, A.R., *Synthesis and characterisation of novel metal pyrophosphates*, 2014, University of Birmingham.

27. Doat, A., F. Pellé, and A. Lebugle, *Europium-doped calcium pyrophosphates: allotropic forms and photoluminescent properties.* Journal of Solid State Chemistry, 2005. **178**(7): p. 2354-2362.
28. Schipper, W., et al., *On the luminescence of hafnium compounds.* Materials research bulletin, 1994. **29**(1): p. 23-30.
29. Assaaoudi, H., I.S. Butler, and J.A. Kozinski, *Crystal structure and vibrational and luminescence spectra of a new erbium potassium pyrophosphate dihydrate, ErK $P_2O_7 \cdot 2H_2O$.* Solid state sciences, 2006. **8**(11): p. 1353-1360.
30. Hizhnyi, Y.A., et al., *The electronic structure and optical properties of AB P_2O_7 (A= Na, Li) double phosphates.* Optical Materials, 2008. **30**(5): p. 687-689.
31. Yuan, J.L., et al., *VUV spectroscopic properties of Ce^{3+} and Pr^{3+}-doped ARE P_2O_7-type alkali rare earth diphosphates (A= Na, K, Rb, Cs; RE= Y, Lu).* Journal of luminescence, 2007. **126**(1): p. 130-134.
32. Kaepe, Z., et al., *Structural and conductivity studies in $LiFeP_2O_7$, $LiScP_2O_7$, and $NaScP_2O_7$.* Journal of Solid State Electrochemistry, 1999. **3**(4): p. 146-152.
33. Ekambaram, S., K. Patil, and M. Maaza, *Synthesis of lamp phosphors: facile combustion approach.* Journal of Alloys and Compounds, 2005. **393**(1-2): p. 81-92.
34. Aruna, S.T. and A.S. Mukasyan, *Combustion synthesis and nanomaterials.* Current opinion in solid state and materials science, 2008. **12**(3-4): p. 44-50.
35. Varma, A., et al., *Solution combustion synthesis of nanoscale materials.* Chemical reviews, 2016. **116**(23): p. 14493-14586.
36. Koch, C., *Synthesis of nanostructured materials by mechanical milling: problems and opportunities.* Nanostructured Materials, 1997. **9**(1-8): p. 13-22.
37. Xia, Y., et al., *Monodispersed colloidal spheres: old materials with new applications.* Advanced Materials, 2000. **12**(10): p. 693-713.
38. Lin, P.-C., et al., *Techniques for physicochemical characterization of nanomaterials.* Biotechnology advances, 2014. **32**(4): p. 711-726.
39. Patel, N.P., et al., *Luminescence study and dosimetry approach of Ce on an α-$Sr_2P_2O_7$ phosphor synthesized by a high-temperature combustion method.* Luminescence, 2015. **30**(4): p. 472-478.
40. Du, F., et al., *Luminescence and microstructures of Eu^{3+}-doped $Ca_9LiGd_{2/3}(PO_4)_7$.* Dalton Transactions, 2011. **40**(43): p. 11433-11440.
41. Mills, A., *Phosphors development for LED lighting.* III-Vs Review, 2005. **18**(3): p. 32-34.
42. Dubey, V., et al., *Effect of Eu^{3+} concentration on photoluminescence and thermoluminescence behavior of YBO_3: Eu^{3+} phosphor.* Superlattices and Microstructures, 2014. **67**: p. 156-171.
43. Page, P. and K. Murthy, *Luminescence associated with Eu^{3+} in two host lattices.* Philosophical Magazine Letters, 2010. **90**(9): p. 653-662.

44. Zhang, Y., W. Gong, and G. Ning, *Novel red-emitting LiGd $(WO_4)_2$: Eu^{3+} phosphor with high thermal stability and high color purity for application in white light-emitting diodes.* New Journal of Chemistry, 2016. **40**(12): p. 10136-10143.
45. Liu, C., J. Liu, and K. Dou, *Judd− Ofelt intensity parameters and spectral properties of Gd_2O_3: Eu^{3+} nanocrystals.* The Journal of Physical Chemistry B, 2006. **110**(41): p. 20277-20281.
46. Huang, J., et al., *Crystal structure, electronic structure, and photoluminescence properties of $La_3BW_{1-x}Mo_xO_9$: Eu^{3+} red phosphor.* Inorganic chemistry, 2014. **53**(18): p. 9541-9547.